Design of Si$_3$N$_4$-based ceramic laminates by the residual stresses

N. ORLOVSKAYA
Drexel University, Philadelphia, PA 19104, USA
E-mail: orlovsk@drexel.edu

J. KUEBLER
EMPA, Swiss Federal Laboratories for Materials Testing and Research,
CH-8600, Duebendorf, Switzerland

V. SUBBOTIN, M. LUGOVY
Institute for Problems of Materials Science, 03142, Kiev, Ukraine

Ceramic laminates with strong interfaces between layers are considered a very promising material for different engineering applications because of the potential for increasing fracture toughness by designing high residual compressive and low residual tensile stresses in separate layers. In this work, Si$_3$N$_4$/Si$_3$N$_4$-TiN ceramic laminates with strong interfaces were manufactured by rolling and hot pressing techniques. The investigation of their mechanical properties has shown that the increase in apparent fracture toughness can be achieved for the Si$_3$N$_4$/Si$_3$N$_4$-20 wt.%TiN composite, while further increase of TiN content in the layers with residual tensile stresses lead to a formation of multiple cracks, and as a result, a significant decrease in the mechanical performance of the composites. Micro-Raman spectroscopy was used to measure the frequency shift across the Si$_3$N$_4$/Si$_3$N$_4$-20 wt.%TiN laminate. These preliminary Raman results can be useful for further analysis of residual stress distribution in the laminate.
© *2005 Springer Science + Business Media, Inc.*

1. Introduction

Ceramics have found their use in numerous crosscutting industrial applications because of excellent hardness, wear, corrosion resistance, and ability to withstand high temperatures. However, ceramics' reliability and ductility compared to metals are not very high. The best approach to increasing the fracture toughness which enables the structural application of ceramics is through the development of ceramic composites. Fiber reinforced composites demonstrate the highest fracture toughness and damage tolerance. However, since these materials have a very high density of weak interfaces, they are not very strong. In addition, their high cost limits their commercial applications. Particulate composites are less expensive to manufacture, but compared to monolithic ceramics, their fracture toughness increases are insignificant. The several publications on ceramics show that the use of layered materials is the most promising method for controlling cracks by deflection, microcracking, or internal stresses [1–3]. Layered structures clearly offer the key to greater reliability at a moderate cost and new applications may result as more complex structures are tailored to specific applications [4].

The way to achieve the highest possible mechanical properties is to control the level of residual stresses in individual layers. One can increase the strength and apparent fracture toughness of ceramics by creating a layer with compressive stresses on the surface. In such a way, surface cracks will be arrested and achieve higher failure stresses [5]. The variable layer composition, as well as the system's geometry, allows the designer to control the magnitude of the residual stresses in such a way that compressive stresses in the outer layers near the surface increase strength, flaw tolerance, fatigue strength, resistance to oxidation, and stress corrosion cracking. In the case of symmetrical laminates, this can be done by choosing layer compositions such that the coefficient of thermal expansion (CTE) of the odd layers is smaller than the CTE of the even ones. The changes in compressive and tensile stresses depend on the mismatch of CTE's, Young's moduli, as well as on the thickness ratio of layers (even/odd). However, if the compressive stresses exist only at or near the surface of ceramics and are not placed inside the material, they will not effectively hinder internal cracks and flaws [6, 7].

It is clear that control over the mechanical behavior and reliability of laminates can be obtained only through design, control of residual stresses, and redistribution of stresses during loading in laminate materials. The sign and value of residual stresses can be established by theoretical prediction. There exists a theoretical background that allows for the design of

laminated ceramics [8]. There have also been a number of experimental studies of laminated ceramics that were conducted using these models, attempting to maximize the mechanical properties.

Silicon nitride is the most promising and well-developed ceramics for structural application because of its outstanding mechanical properties as well as its superior wear resistance [9]. The addition of TiN to Si_3N_4 leads to an increase of Young's modulus, electrical conductivity, and CTE of Si_3N_4 ceramics [10]. By varying the amount of TiN in silicon nitride ceramics, we can increase the CTE/Young's modulus mismatch and develop composites with compressive and tensile stresses in alternative layers. This may further improve the mechanical properties of laminates [11–13]. β-Si_3N_4 belongs to the space group C^2_{6h} ($P6_3$/m) and the irreducible representation for the optical phonons has been reported [14–17]

$$\Gamma_{optic} = 4A_g + 2A_u + 3B_g + 4B_u + 2E_{1g} + 5E_{2g} + 4E_{1u} + 2E_{2u}$$

where A_g, E_{1g} and E_{2g} modes are Raman active and A_u and E_{1u} are infrared active. Raman and infrared active bands are mutually excluded since the crystal structure has a center of symmetry.

The goal of this work is to study the interrelation between structure, residual stresses, mechanical properties, and fracture behavior of complex particulate-layered Si_3N_4/Si_3N_4-TiN based composites.

2. Analysis of residual stresses

In this work, two-component brittle layered composites with symmetric macrostructure are considered. The layers consisting of different components alternate one after another, but the external layers consist of the same component. Thus, the total number of layers N in such a composite sample is odd. The layers of the first component including two external (top) layers are designated by index 1 ($j = 1$), and the layers of the second component (internal) are designated by index 2 ($j = 2$). The number of layers designated by index 1 is $(N+1)/2$ and the number of layers designated by index 2 is $(N-1)/2$. The layer of each component has some constant thickness, and the layers of same component have identical thickness.

There are effective residual stresses in the layers of each component in the layered ceramic composite. During cooling, the difference in deformation due to the different thermal expansion factors of the components is accommodated by creep as long as the temperature is high enough. Below a certain temperature, which is called the "joining" temperature, the different components become bonded together and internal stresses appear. In each layer, the total strain after sintering is the sum of an elastic component and a thermal component [18]. In the case of a perfectly rigid bonding, the residual stresses in the layers of a two-component

material are [19]:

$$\sigma_{r1} = \frac{E'_1 E'_2 f_2 (\alpha_{T2} - \alpha_{T1})\Delta T}{E'_1 f_1 + E'_2 f_2} \qquad (1)$$

and

$$\sigma_{r2} = \frac{E'_2 E'_1 f_1 (\alpha_{T1} - \alpha_{T2})\Delta T}{E'_1 f_1 + E'_2 f_2} \qquad (2)$$

where $E'_j = E_j/(1 - v_j)$, $f_1 = \frac{(N+1)l_1}{2h}$, $f_2 = \frac{(N-1)l_2}{2h}$, E_j and V_j is the elastic modulus and Poisson's ratio of j-th component respectively, l_1 and l_2 are the thickness of layers for the first and second component, α_{T1} and α_{T2} are the thermal expansion coefficients (CTE) of the first and second components respectively, ΔT is the difference between the joining temperature and the current temperature, and h is the total thickness of the specimen.

The choice of composition for Si_3N_4-based ceramic laminates is dependent on the coefficient of thermal expansion and Young's modulus of the compounds. Four compositions of composite layers were used:

1. Si_3N_4-5 wt.% Y_2O_3-2 wt.% Al_2O_3;
2. TiN;
3. Si_3N_4 (5 wt.%Y_2O_3-2 wt.%Al_2O_3)-20 wt.%TiN;
4. Si_3N_4 (5 wt.% Y_2O_3-2 wt.% Al_2O_3)-50 wt.%TiN.

The residual stresses in each layer of the Si_3N_4/Si_3N_4-20%TiN, Si_3N_4/Si_3N_4-50%TiN, and Si_3N_4/TiN laminates, each sample having different numbers of layers and known layer thickness, were calculated using Equations 1 and 2 [19]. The joining temperature, used to determine the residual stresses, was assumed to be 1200 °C rather than the hot pressing temperature of 1800 °C. It was found that these materials are sufficiently soft at the temperature above 1200 °C to have a zero stress state due to ductile glassy phases at the grain boundaries. Young's moduli and CTE's of the components were calculated by the rule of mixture and are presented in Table I. Results of the residual stress calculations are shown in Table II.

3. Experimental
α-Si_3N_4 ($d_{50} = 1\ \mu m$) and TiN ($d_{50} = 3\ \mu m$) was used for mixture preparation. Grinding of mixtures of certain compositions was done in the ball mill for 5 h. After grinding, the plastification and rolling of thin tapes was

TABLE I Young's moduli and CTE of the components

Composition	E, GPa	CTE, 1/K
Si_3N_4-5 wt.% Y_2O_3-2 wt.% Al_2O_3	320	3×10^{-6}
TiN	440	9.35×10^{-6}
Si_3N_4(5 wt.% Y_2O_3-2 wt.%Al_2O_3)-20 wt.% TiN	335.62	3.826×10^{-6}
Si_3N_4(5 wt.% Y_2O_3-2 wt.% Al_2O_3)-50 wt.%TiN	364.93	5.378×10^{-6}

Composition	Thickness of layers (μm)		$\sigma_{com.}$ (MPa)	$\sigma_{tens.}$ (MPa)
	Si_3N_4	Si_3N_4 with TiN		
Si_3N_4/Si_3N_4— 20 wt.%TiN	250	210	188	246.5
$Si_3N_4/2(Si_3N_4$— 20 wt.%TiN)	245	530	279.5	151
Si_3N_4/Si_3N_4— 50 wt.%TiN	200	330	765	515.5
Si_3N_4/TiN	200	400	2467	1078

done. For rolling, a crude rubber (4 wt.%) was added to the mixture of powders as a plasticizer through a 3% solution in petrol. The powders were then dried up to a 2 wt.% residual amount of petrol in the mixture. After sieving powders with a 500 μm sieve, granulated powders were dried up to the 0.5 wt.% residual petrol. A roll mill with 40 mm rolls was used for rolling. The velocity of rolling was 1.5 m/min. Working pressure varied from 10 MPa for a 64% relative density of tapes to 100 MPa for a 74% relative density. The thickness of tapes was either 0.4–0.5 mm or 0.8–1.0 mm, the width was 60–65 mm. Samples of ceramics were prepared by the hot pressing of tapes stacked together. Each layer contained one or a few tapes. Graphite dies were used for hot pressing, and the hot pressing was performed at a temperature of 1820 °C, with a dwelling time of 20 min and a pressure of 30 MPa [20]. During hot pressing, the shrinkage of layers occurred 3 times such that after rolling, the thickness of the individual tape was 450 μm, while after hot pressing it decreased to 150 μm. After hot pressing, the thickness of the Si_3N_4 layers was in the range of 150–300 μm, and the thickness of the Si_3N_4 layers with TiN additive varied from 200 to 500 μm.

Fracture toughness was also measured by Single-Edge-V-Notched-Beam (SEVNB) method [21]. 4-point bending strength of the machined specimens was determined using a jig with an inner span of 20 mm and an outer span of 40 mm. The notch tip was located in a second Si_3N_4 layer in the case of layered composites. Strength and Young's modulus were also calculated at room temperature by measuring the deflection of samples during 4-point bending tests according to the standard. The bending strength calculation was based on a monolithic sample analysis. Optical and scanning electron microscopy was used for a microstructure investigation.

A Renishaw 1000 Raman microspectrometer was equipped with a Leica microscope, an XYZ mapping stage and 514.5 nm argon ion laser. The laser generated 12.5 mW of power. A plasma filter was used to remove plasma lines from the spectra taken. The laser spot was about 1–2 μm for the 100 × objective lens used during the measurements. Autofocusing was used to collect the Raman spectra because it maintains a good focus on the sample during line mapping experiments. The system was set up to take spectra from all points along a single line of interest on the surface. Before the Si_3N_4 measurements, the spectrometer was calibrated using a standard Si wafer band with position at 520.3 cm^{-1}.

4. Results and discussion
4.1. Mechanical properties

Mechanical properties such as the strength, Young's modulus, and fracture toughness of the laminates are presented in Table III. The parameters of the tested laminates, such as composition and layer thickness are given in Table II. Besides these four designs, one more design of Si_3N_4/Si_3N_4 laminate was used as a base for comparison. The laminates of this design were prepared in the same way as the others, however, all layers were of the same composition. Therefore, no residual stresses can appear during cooling. It is worth noting that both the Young's modulus and fracture toughness of these Si_3N_4/Si_3N_4 laminates were measured to be on the same level as standard Si_3N_4 ceramics prepared by the standard powder route, which includes no rolling. The strength of the Si_3N_4/Si_3N_4 laminate was less than that of the standard Si_3N_4 ceramics with values of 507.6 ± 3.2 and 750 ± 20.7 MPa, respectively. As one can see from Table III, while the strength of Si_3N_4/Si_3N_4-20wt.% TiN laminates are approximately on the same level as the Si_3N_4/Si_3N_4 laminates, further increase of the TiN content to 50 and 100% results in a significant decrease of both strength and Young's modulus. The measured fracture toughness of the Si_3N_4/TiN laminates also showed a decrease similar to strength and Young's modulus values.

The Si_3N_4/Si_3N_4-20 wt.% TiN laminates showed an increase in apparent fracture toughness. This increase can be explained by the introduction of the residual bulk compressive stresses in Si_3N_4 layers. In the case where the thicknesses of the Si_3N_4 and the Si_3N_4-20 wt.% TiN layers were similar, the calculated residual compressive stress was about 188 MPa and the residual tensile stress about 246.5 MPa. The measured value of the apparent fracture toughness was 7.41 ± 1.79 MPa m$^{1/2}$. There was a further increase in K_{Ic} (8.5 ± 0.01 MPa m$^{1/2}$) for the laminates with 20 wt.%TiN when the relative thickness of the Si_3N_4-20 wt.%TiN layers was increased compared to the thickness of pure Si_3N_4 layers. The reason for this is a significant increase of the residual compressive stress, and at the same time, a decrease of the residual stress in the Si_3N_4-20 wt.% TiN layers (Table II). However, an increase of TiN content to 50 wt.% resulted in a significant increase of the residual tensile stress in the laminates. The calculated tensile stress val-

Composition	σ_f (Mpa)	E (GPa)	K_{IC} (MPa·m$^{1/2}$)
Si_3N_4/Si_3N_4	507.6 ± 3.2	306.6	5.54 ± 0.01
Si_3N_4/Si_3N_4- 20 wt.%TiN	356.2 ± 76.4	312.9	7.41 ± 1.79
$Si_3N_4/2(Si_3N_4$- 20 wt.%TiN)	450.4 ± 82.9	–	8.5 ± 0.01
Si_3N_4/Si_3N_4- 50 wt.%TiN	157.9 ± 14.9	297.7	–
Si_3N_4/TiN	140.8 ± 10.9	157.4	3.97 ± 0.52

ues are higher than the tensile strength of the material, and therefore there is much cracking and a decrease in all mechanical properties.

4.2. Fracture surfaces

The typical fracture surfaces of pure Si_3N_4 layer and Si_3N_4-20 wt.%TiN layer are shown in Fig. 1. The bimodal grain size distribution exists with a number of elongated grains being surrounded by small rounded grains of Si_3N_4 (Fig. 1a). The average grain size in the Si_3N_4 layer was 0.4–0.5 μm. The micrograph of the Si_3N_4-20%TiN fracture surface revealed that a majority of the grain sizes were in the range of 1–2 μm, with some grains of a size less than 1 μm (Fig. 1b). It was shown that the TiN has a homogeneous distribution in the Si_3N_4 matrix and no solid solution was detected between Si_3N_4 and TiN particles [22].

Fracture surfaces of Si_3N_4/Si_3N_4, Si_3N_4/Si_3N_4-20 wt.%TiN, $Si_3N_4/2(Si_3N_4$-20 wt.%TiN) and $Si_3N_4/$ TiN laminates are shown in Fig. 2. $2(Si_3N_4$-20 wt.%TiN) means that thickness of (Si_3N_4-20 wt.%TiN) layer is twice than that of Si_3N_4 layer. The fracture surface of the Si_3N_4/Si_3N_4 laminate, where no residual stresses were generated during cooling, is flat and smooth (Fig. 2A). As layers of different composition are used, the fracture surface becomes rougher. For the Si_3N_4/Si_3N_4-20 wt.%TiN laminate, there are two zones on the fracture surface. The first zone near the notch tip has a rough surface and corresponds to a slow crack growth. The second zone has a rather smooth surface with distinct steps only at the interfaces between layers. This zone corresponds to a fast crack growth (Fig. 2B). No crack bifurcation occurred and two equal parts of the sample could be found after failure. The $Si_3N_4/2(Si_3N_4$-20 wt.%TiN) laminates failed after crack bifurcation. The part of the fracture surface near the notch tip was the same as the ones shown in Fig. 1A and B. At the moment when the crack bifurcated, an unusually smooth fracture surface was observed (Fig. 2C). When the value of residual tensile stresses approaches the value of the tensile strength of the layer, cracks in the layers are generated, as was the case of the Si_3N_4/Si_3N_4-50 wt.%TiN and Si_3N_4/TiN laminates. The cracks originated during the cooling stage after the hot pressing of the laminates and appeared due to mismatching of CTEs and elastic moduli of two different layers. Channel cracks were observed in the laminates with a difference in composition between layers, starting with 50 wt.%TiN content and higher. Si_3N_4/TiN laminates demonstrate channel cracking (Fig. 2D) similar to the cracks described in [23]. These cracks are responsible for the dramatic decrease in the mechanical properties of Si_3N_4 based laminates. To reduce or eliminate cracking, it is necessary to make composites with characteristics more close between layers, especially the CTE and elastic moduli. The extent of channel cracking was decreased in laminates with Si_3N_4-50 wt.%TiN layers in comparison to composites where one of the layers was pure TiN. Channel cracking was fully eliminated for composites with a Si_3N_4-20 wt.%TiN layer composition. An absence of pre-existent cracks resulted in an increase of the strength and fracture toughness.

The fracture surface of Si_3N_4/Si_3N_4-50 wt.% TiN is shown in Fig. 3. As one can see, there is a high roughness of the surface, and bifurcation of the moving crack occurred when it was inside the Si_3N_4 layer with residual compressive stresses. There are fracture steps and channel cracks at the Si_3N_4-50 wt.%TiN layers which are perpendicular to the interfaces of composite. The fracture steps appeared only at layers with tensile stresses. Such fracture steps and other defects are responsible for a decrease in mechanical properties. Multiple bifurcations occur for preexisting cracks inside the layers with residual compressive stresses, and, in addition, the moving crack bifurcates during the sample loading. The schematic presentation and an optical image of the crack bifurcation during the failure of this laminate are shown in Fig. 4.

4.3. Raman shift measurements

A measurement of residual stresses is an important issue in the development of the laminates. A number of works have been published which use Raman spectroscopy for the determination of residual stresses. Strengthening arising from the residual stresses in Al_2O_3/ZrO_2 composites has been evaluated [24]. The magnitude of bridging stresses in Si_3N_4 and Al_2O_3

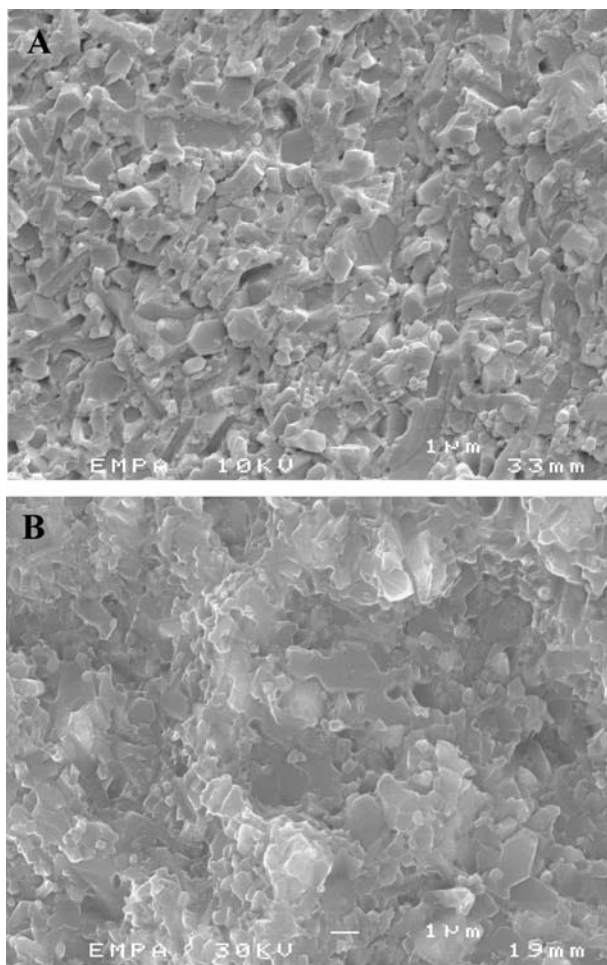*Figure 1* Micrographs of fracture surfaces of Si_3N_4 layer (A) and Si_3N_4-20 wt.%TiN layer (B) in Si_3N_4/Si_3N_4-20 wt.%TiN laminate.

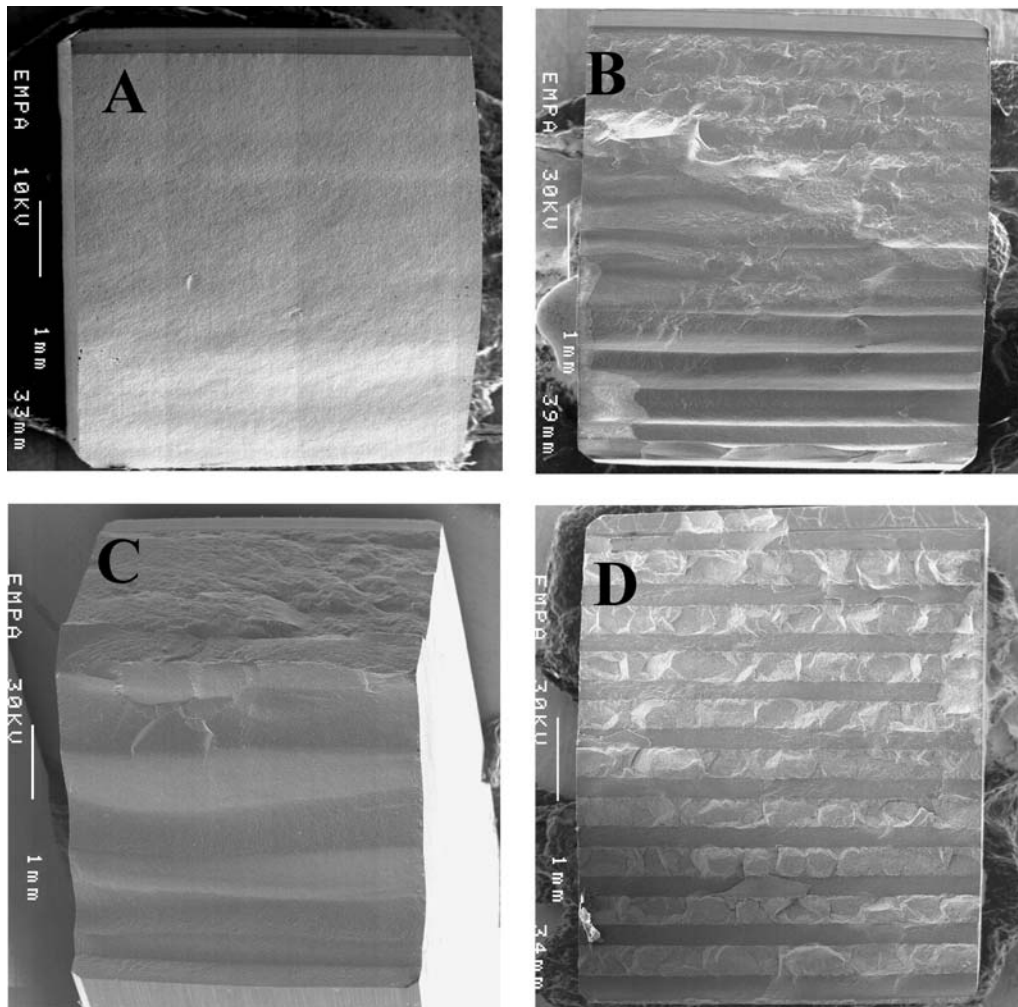*Figure 2* Fracture surface of laminate composite. (A) Si_3N_4/Si_3N_4 laminates; (B) Si_3N_4/Si_3N_4-20 wt.%TiN laminates; (C) $Si_3N_4/2(Si_3N_4$-20 wt.%TiN) laminates and (D) Si_3N_4/TiN laminates.

during crack propagation has also been estimated [25, 26]. Some attempts to use Raman spectroscopy to estimate the residual stresses around indentation in silicon nitride have been done [27, 28], but the results were contradictive and further clarification is needed. The determination of residual stress in laminates is a complicated problem. Here we report the preliminary results of the Raman shift measurements that can be further used to estimate the residual stresses in a laminar composite.

Two typical Si_3N_4 Raman spectra are shown in Fig. 5. The spectrum in Fig. 5a was taken at the center of a thin Si_3N_4 layer from the side face of the $Si_3N_4/2(Si_3N_4$-20 wt%TiN) laminate. The thickness of Si_3N_4 layer was about 250 μm and the thickness of Si_3N_4-20 wt%TiN layer was about 500 μm. A first indication of existing tensile mean stress came from the shift of the Si band to 518 cm^{-1} because the spectrometer was calibrated with a Si band being at 520.3 cm^{-1} at the beginning of experiment. Free Si can sometimes be detected in Si_3N_4 as a result of desublimation of Si_3N_4. The band positions of unstressed Si_3N_4 were determined as 181, 203, 224, 446, 615, 728, 862, 926, 936, 1044 cm^{-1}. Also, Si_3N_4 bands 862 cm^{-1}, 1044 cm^{-1}, and others are shifted to lower wavenumbers in the center of a thin Si_3N_4 layer. Three strong bands (181, 203, 224 cm^{-1}) did not change their positions relative to the unstressed Si_3N_4,

however. The spectrum in Fig. 5b was taken from the center of a Vickers indentation (20 kg load) placed in the center of a thin Si_3N_4 layer from the same face of $Si_3N_4/2(Si_3N_4$-20%TiN) laminate. The first three bands remain intact, but the other bands shifted to the higher wave numbers, which indicates the existence of a residual compressive stress in the center of the Vickers impression induced by the indentation. These results are similar to published results [27, 28].

One-dimensional maps of band shift, band intensity, FWHM, and other band parameters can be produced using a line scan technique [29]. Line mapping of the 862 cm^{-1} Raman band of silicon nitride was performed across a thin Si_3N_4 layer from the $Si_3N_4/2(Si_3N_4$-20%TiN) laminate, starting at the Si_3N_4-20% TiN layer, crossing the interfaces, and ending in the next Si_3N_4-20%TiN layer (Fig. 6). Maps of intensity (Fig. 6A), FWHM (Fig. 6B), and peak shift (Fig. 6C) were generated. As one can see, there is a shift in peak position from 862.54 cm^{-1} in the Si_3N_4-20%TiN layer to 861.05 cm^{-1} in the pure Si_3N_4 layer (Fig. 6C). Similar results have been published in [30]. The shift exists because of different surface stress states in layers with different composition [31–33]. There is tensile mean stress on the surface of the Si_3N_4 layers, since a down shift of the peak position was found. At the same time, a compressive mean stress
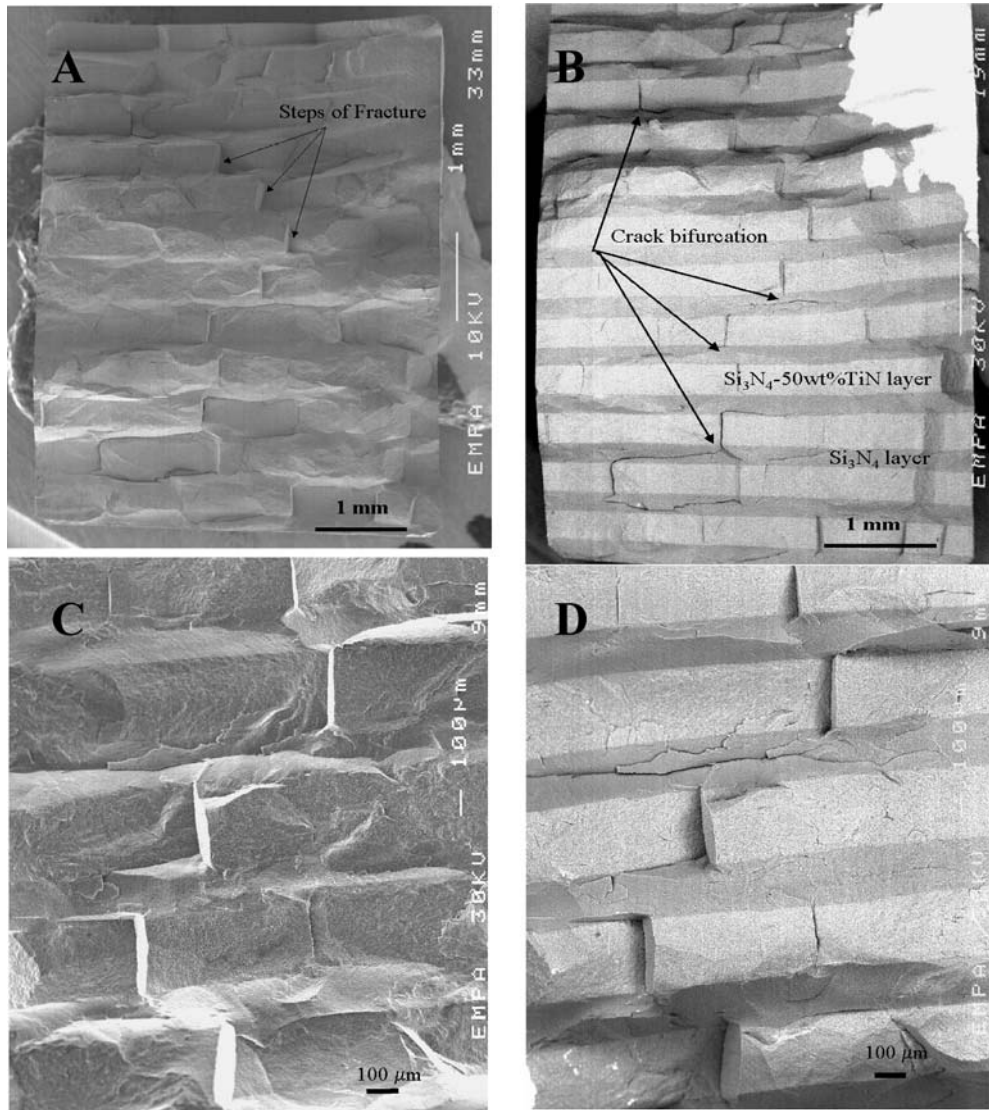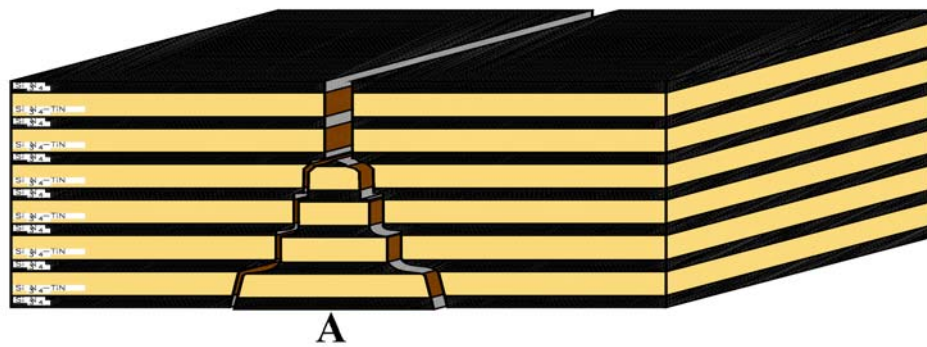
Figure 3 Fracture surface of Si$_3$N$_4$/Si$_3$N$_4$-50% wt.%TiN composite. (A) and (C) SEI image; (B) and (D) backscattered image.
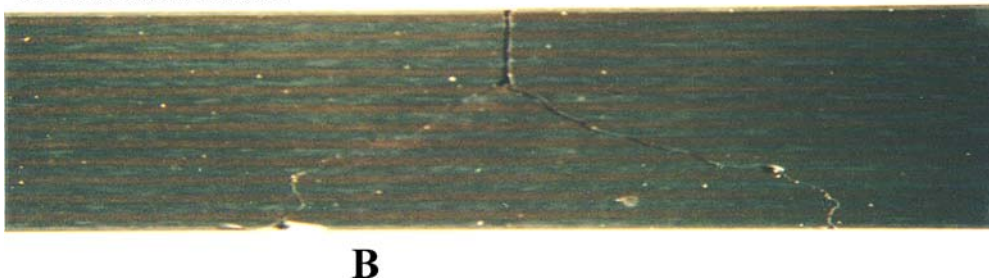
Figure 4 (A) A schematic drawing of a crack bifurcation during the fracture in Si$_3$N$_4$/Si$_3$N$_4$-TiN laminates; (B) An optical photograph of the Si$_3$N$_4$/Si$_3$N$_4$-50 wt.%TiN laminate bar after fracture.
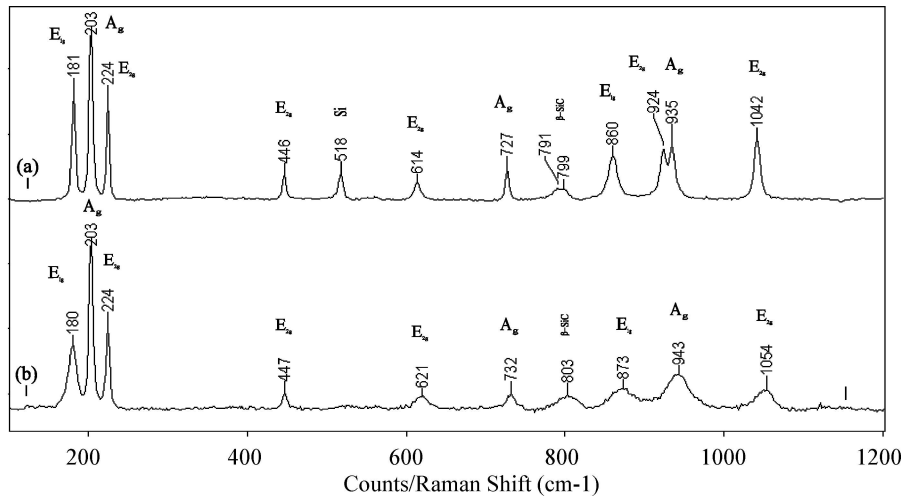
Figure 5 Positions of Raman bands of Si_3N_4 in the center of (a) thin Si_3N_4 layer with surface tensile stresses and (b) Vickers impression. Load is 20 kg.
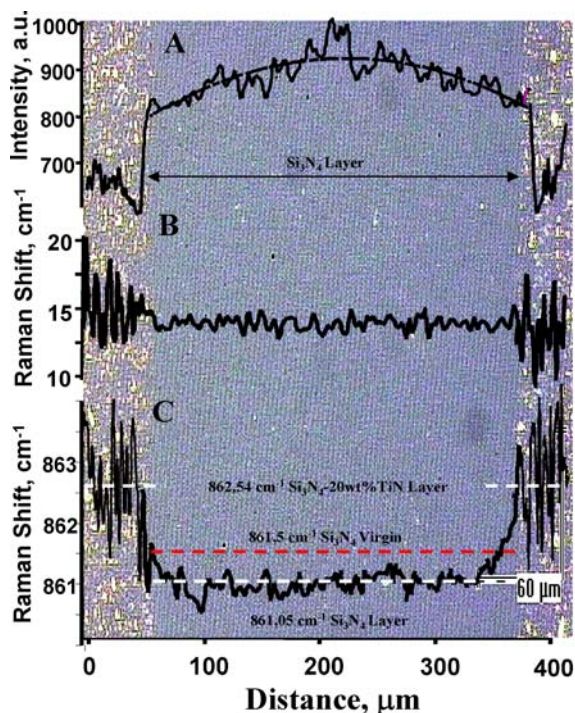

Figure 6 862 cm^{-1} band line mapping across Si_3N_4 Layer. (A) A peak intensity map; (B) A FWHM map; (C) A peak shift map.

exists on the Si_3N_4-20 wt.% TiN surface. Since the expansion coefficient of the Si_3N_4 is lower than that of the Si_3N_4-TiN, therefore, after cooling we have bulk residual compressive stress in the Si_3N_4 layer and bulk residual tensile stress in the Si_3N_4-TiN layer. However, edge effects appear on a side face of the layered sample. Edge tensile stress exists on side surface of the Si_3N_4 layer and edge compressive stress appears on a side surface of the Si_3N_4-TiN layer. Raman shift depends on the sum of bulk and edge components of stress with edge components dominating on a side face. In such a way Raman shift indicates the presence of a tensile surface stress in Si_3N_4 layer and compressive surface stress in Si_3N_4-TiN layer.

The FWHM map reveals a large scatter of the 862 cm^{-1} peak in Si_3N_4-20 wt.%TiN layer (Fig. 6b). This is partially because of the TiN second phase, which

influences the intensity of the Raman signal, and partially because Si_3N_4 is under less uniform compressive microstresses in the Si_3N_4-20 wt.%TiN layer, as compared to pure Si_3N_4. The intensity scan of the 862 cm^{-1} band reveals a strong maximum in the center of Si_3N_4 layer (Fig. 6a). These preliminary results can be useful for further analysis of residual stress distribution in the laminate.

5. Conclusions

Si_3N_4 based multilayered ceramics with layers of different thickness and compositions were manufactured by rolling and hot pressing techniques. The compositions and thickness of layers varied to design residual compressive and tensile stresses which affected the mechanical behavior of the composite. The increase of apparent fracture toughness (8.5 ± 0.01 MPa m$^{1/2}$) was achieved when the residual compressive stress in pure Si_3N_4 layers was equal to 280 MPa, but at the same time the residual tensile stress in Si_3N_4-20 wt.%TiN layers was 150 MPa. When the amount of TiN was increased to 50wt.% or 100%, multiple cracks appeared in the layers with a residual tensile stress, which lead to the degradation of the mechanical properties. Numerous crack bifurcations were observed after the failure of the Si_3N_4/Si_3N_4-50 wt.%TiN laminates. A bifurcation of the moving crack has also occurred during the failure of Si_3N_4/2(Si_3N_4-20 wt.%TiN) laminates. Micro-Raman spectroscopy was used for Raman shift measurements, and preliminary results have revealed that tensile mean stress exists on the surface of Si_3N_4 layers, which have residual compressive stress in the bulk. At the same time, compressive mean stress exists on the surface of Si_3N_4-20 wt.%TiN layers, which have residual tensile stress in the bulk. Further work is required to estimate quantitatively the magnitude of the surface residual stresses identified by the micro-Raman spectroscopy.

5449

References

1. W. J. CLEGG, *Science* **286** (1999) 1097.
2. W. J. CLEGG, K. KENDALL, N. ALFORD, T. W. BUTTON, and J. D. BIRCHALL, *Nature* **347** (1990) 455.
3. M. P. RAO, A. J. SANCHEZ-HERENCIA, G. E. BELTZ, R. M. MCMEEKING and F. F. LANGE, *Science* **286** (1999) 102.
4. H. CHAN, *Ann. Rev. Mater. Sci.* **27** (1997) 249.
5. P. HONEYMAN-CLOVIN and F. F. LANGE, *J. Am. Ceram. Soc.* **79** (1996) 1810.
6. M. OECHSNER, C. HILLMAN and F. F. LANGE, *ibid.* **79** (1996) 1834.
7. A. SANCHEZ-HERENCIA, C. PASCUAL, J. HE and F. LANGE, *ibid.* **82** (1999) 1512.
8. C. A. FOLSOM, F. W. ZOK and F. F. LANGE, *ibid.* **77** (1994) 689.
9. F. L. RILEY, *ibid.* **83** (2000) 245.
10. Y. GOGOTSI, *J. Mater. Sci.* **29** (1994) 2541.
11. P. SAJGALIK, Z. LENCES and J. DUSZA, *ibid.* **31** (1996) 4837.
12. V. YAROSHENKO, N. ORLOVSKAYA, M.-A. EINARSRUD, K. BERROTH and V. KOVYLAYEV, *Key Eng. Mater.* **132–136** (1997) 2017.
13. T. OHIJ, L. SHIEGEGAKI, T. MIYAJIMA and S. KANZAKI, *J. Am. Ceram. Soc.* **80** (1997) 991.
14. N. WADA, S. A. SOLIN, J. WONG and S. PROCHAZKA, *J. Non-Cryst. Solids* **43** (1981) 7.
15. K. HONDA, S. YOKOYAMA and S. TANAKA, *J. Appl. Physics* **85** (1999) 7380.
16. J. DONG and O. SANKEY, *ibid.* **87** (2000) 958.
17. A. TAKASE and E. TANI, *J. Mater. Sci. Lett.* **6** (1987) 607.
18. T. CHARTIER, D. MERLE and J. L. BESSON, *J. Europ. Ceram. Soc.* **16** (1995) 101.
19. M. LUGOVY, N. ORLOVSKAYA, K. BERROTH and J. KUEBLER, *Comp. Sci. Technol.* **59** (1999) 1429.
20. V. YAROSHENKO, N. ORLOVSKAYA, M.-A. EINARSRUD and V. KOVYLAYEV, in Proceedings of NATO ARW " Multilayered and Fibre-Reinforced Composites: Problems and Prospects", edited by Y. M. Haddad (Kluwer, Dordrech, 1998) p. 285.
21. J. KUEBLER, ASTM STP 1409, J. A. Salem, edited by M. G. Jenkins and G. D. Quinn, ASTM, West Conshohocken, PA, USA, ISBN 0-8031-2880-0, (2002) p. 93.
22. N. ORLOVSKAYA, V. SUBBOTIN and M. LUGOVY, unpublished work.
23. N. BAI, D. D. POLLARD and H. GAO, *Nature* **403** (2000) 753.
24. G. PEZZOTTI, V. SERGO, O. SBAIZERO, N. MURAKI, S. MERIANI and T. NISHIDA, *J. Erop. Ceram. Soc.* **19** (1999) 247.
25. G. PEZZOTTI, N. MURAKI, N. MAEDA, K. SATOU and T. NISHIDA, *J. Am. Ceram. Soc.* **82** (1999) 1249.
26. G. PEZZOTTI, H. SUENOBU, T. NISHIDA and O. SBAIZERO, *ibid.* **82** (1999) 1257.
27. N. MURAKI, G. KATAGIRI, V. SERGO, G. PEZZOTTI and T. NISHIDA, *J. Mater. Sci.* **32** (1997) 929.
28. V. SERGO, G. PEZZOTTI, G. KATAGIRI, N. MURAKI and T. NISHIDA, *J. Am. Ceram. Soc.* **79** (1996) 5419.
29. M. BOWDEN, *Appl. Spectr.* **51** (1997) 1405.
30. N. ORLOVSKAYA and Y. GOGOTSI, Euro Ceramics VII, PT 1-3, *Key Eng. Mater.* **206**(2), (2002) 1025.
31. V. SERGO, D. M. LIPKIN, G. DE PORTU and D. R. CLARKE, *J. Am. Ceram. Soc.* **80** (1997) 1633.
32. S. HO, C. HILLMAN, F. F. LANGE and Z. SUO, *J. Am. Ceram. Soc.* **78** (1995) 2353.
33. N. L. HARRISON and W. J. HARRISON, *J. Adhes.* **3** (1972) 195.